Journal of Engineering, Project, and Production Management
2026, 16(5), 2026-0056

A Machine Learning-Based Temperature Monitoring Method for Power Equipment by Fusing Morphological Features and Chromaticity Analysis

Yuze Chen[1], Shanyi Xie[2], Kai Zhang[3], Ying Fan[4], and Gang Zhou[5]
[1] Engineer, Electric Power Research Institute of Guangdong Power Grid Co., Ltd., China, E-mail: chenyuze@dky.gd.csg.cn (corresponding author).
[2] Senior Engineer, Electric Power Research Institute, Guangdong Power Grid Co., Ltd., China, E-mail: xieshanyi@dky.gd.csg.cn
[3] Engineer, Electric Power Research Institute, Guangdong Power Grid Co., Ltd., China, E-mail: zhangkai@dky.gd.csg.cn
[4] Senior Engineer, Electric Power Research Institute, Guangdong Power Grid Co., Ltd., China, E-mail: fanying@dky.gd.csg.cn
[5] Senior Engineer, Electric Power Research Institute, Guangdong Power Grid Co., Ltd., China, E-mail: zhougang@dky.gd.csg.cn

Project Management
Received May 12, 2026; revised June 7, 2026; July 10, 2026; accepted July 13, 2026
Available online July 25, 2026

Abstract: A bi-level deep reinforcement learning-based, geographically digitized, thermal-state-aware energy coordination framework is proposed to address the limitation that temperature monitoring is typically treated as an external diagnostic rather than a control variable. The model embeds aerial electric-drone temperature monitoring, morphological features, and chromaticity analysis directly into the dispatch logic within a thermally coupled green energy hub-aerial e-drone charging system. A hierarchical Feudal Reinforcement Learning structure supported by the twin delayed deep deterministic policy gradient co-optimizes generation priority, cost reduction, and inspection strategy under uncertainty. Results show a mean daily operating cost reduction of 8 % compared with the twin delayed deep deterministic policy gradient and 15 % relative to the distributed distributional deep deterministic policy gradient, remaining within 5 % of the optimal solution obtained using a perfect mixed-integer linear programming solution. Over 100 days, coordinated drone-enabled energy exchange decreases total expenditure by 9 %. Full feature-based monitoring reduces the integrated cost by more than 11% and the Thermal Risk Index by 61%. Forced combined heat and power derating events decrease from 47 to 12, while inspection coverage reaches 96 %.

Keywords: Deep reinforcement learning; temperature monitoring; geographically digitalized energy coordination; thermal-state-aware.

DOI 10.32738/JEPPM-2026-0056

---

1. Introduction

Green Energy Hubs (GEHs) have emerged as an effective solution for integrating electricity, heating, cooling, renewable generation, energy storage, and flexible electrical loads within a unified energy management framework (Zhang et al., 2025). By coordinating multiple energy carriers, GEHs improve energy efficiency, renewable energy utilization, and operational flexibility (Franzoso et al., 2026). However, the increasing penetration of renewable energy sources, bidirectional power exchange, and mobile electric resources introduces significant operational uncertainty that cannot be effectively addressed by conventional cost-oriented dispatch strategies (Shayeghi et al., 2026). In addition to economic considerations, the thermal condition of critical equipment directly influences operating efficiency, available generation capacity, equipment lifetime, and system reliability (Wang et al., 2025; Kardaris et al., 2025). Nevertheless, equipment temperature is generally monitored only for maintenance purposes and is rarely incorporated into real-time operational decision-making. Furthermore, aerial inspection data obtained from mobile sensing platforms introduce additional spatial and temporal uncertainty, making the coordination of inspection and energy dispatch considerably more challenging (Andreou et al., 2023; Bansal et al., 2023).

Recent advances in reinforcement learning have significantly improved the capability of integrated energy systems to perform adaptive scheduling under uncertainty. Hierarchical and deep reinforcement learning architectures have demonstrated promising performance in economic dispatch and operational coordination of multi-energy systems. Luo and

Jiang (2025) proposed a hierarchical deep reinforcement learning framework for coordinated energy management, while Franzoso et al. (2026) integrated mixed-integer linear programming with Twin Delayed Deep Deterministic Policy Gradient (TD3) to improve industrial multi-energy control. Multi-agent reinforcement learning has further been applied to coordinated scheduling of integrated energy systems, hydrogen storage, electric vehicles, and peer-to-peer energy transactions (Shayeghi et al., 2026; Zhang et al., 2025; Li et al., 2025; Shayeghi et al., 2026; Toquica et al., 2025; Mohamadi et al., 2025a). Additional studies have incorporated degradation-aware optimization, carbon trading, safe reinforcement learning, and robust scheduling under uncertainty (Qi et al., 2025; Bashyal et al., 2025; Deng et al., 2025; Li et al., 2025; Kardaris et al., 2025; Zhou et al., 2025). Although these approaches improve economic performance and operational robustness, thermal constraints are generally represented using simplified degradation models/predefined operating limits rather than real-time equipment condition obtained through field inspection.

Alongside advances in reinforcement learning for energy scheduling, considerable progress has also been achieved in condition-based inspection and maintenance decision-making, where equipment health information is directly utilized to optimize operational policies. Wei et al. (2026) developed a belief-based Semi-Markov Decision Process (SMDP) framework for predictive inspection and maintenance of multi-state systems, demonstrating that dynamically updated health-state information significantly improves maintenance decisions compared with conventional periodic inspection strategies. Wei et al. (2024) further investigated fleet service reliability using a two-dimensional inspection and maintenance policy, showing that inspection outcomes substantially influence system availability and long-term operational reliability in distributed service systems. More recently, Wei and Cheng (2025) proposed an optimal maintenance framework for self-service systems subject to competing sudden and deterioration-induced failures, highlighting the importance of integrating real-time condition information into sequential operational decision-making under uncertainty. Collectively, these studies demonstrate an important shift from schedule-based maintenance to condition-informed operational decision-making, in which inspection-derived system health actively guides operational actions rather than merely supporting post-fault maintenance.

Complementary to these advances in condition-informed maintenance, parallel developments in intelligent inspection technologies have substantially improved the acquisition of equipment health information for power systems. Infrared thermography, image enhancement, feature fusion, and deep learning techniques enable accurate detection and localization of thermal anomalies before severe equipment degradation occurs. Wang et al. (2025) reviewed recent advances in infrared thermography for intelligent inspection, while Zhang et al. (2023), Li et al. (2025), and Chen et al. (2025) improved thermal image interpretation through image enhancement, federated learning, and multimodal feature extraction. Recent studies have also demonstrated the effectiveness of Unmanned Aerial Vehicles (UAVs) for geographically distributed inspection. Andreou et al. (2023) developed an efficient UAV trajectory optimization approach for smart-city applications, whereas Bansal et al. (2023) investigated coordinated UAV communication under uncertain channel conditions. These studies demonstrate the growing capability of aerial platforms for autonomous monitoring of geographically distributed infrastructure. However, existing inspection systems primarily treat thermal information as diagnostic evidence for maintenance planning and fault detection, while the extracted temperature distributions, morphological characteristics, and chromaticity information remain largely disconnected from reinforcement learning-based operational control.

Consequently, an important research gap exists between intelligent inspection and intelligent energy management. Existing learning-based scheduling frameworks optimize energy dispatch using electrical, economic, and renewable generation information, but do not consider real-time equipment condition, whereas infrared inspection systems identify thermal abnormalities primarily for fault diagnosis, condition assessment, or maintenance planning, without influencing operational decisions. As a result, valuable inspection-derived thermal information remains isolated from the scheduling process, preventing dispatch strategies from adapting dynamically to equipment health and thermal risk. Although reinforcement learning for energy scheduling, infrared thermography for equipment inspection, and hierarchical control architectures have each been extensively investigated, these research directions have largely evolved independently. To the best of the authors' knowledge, no existing study has established a unified framework that directly integrates geographically digitalized aerial thermal inspection with reinforcement learning-based energy management by embedding inspection-derived thermal information into the scheduling state, reward mechanism, and operational feasibility constraints.

To address this gap, this study proposes a bi-level, geographically digitalized, thermally adaptive energy coordination framework for a GEH integrated with an Aerial e-drone Charging System (AEDCS). The proposed framework builds upon established reinforcement learning algorithms, infrared thermographic inspection techniques, and hierarchical control concepts reported in previous studies; however, its technical contribution lies in the unified integration of these elements for condition-aware operational coordination. Specifically, infrared-derived temperature information, together with the Morphological Deviation Index (MDI) and Chromaticity Anomaly Score (CAS) extracted from AED inspection, is incorporated directly into the reinforcement learning state representation, reward formulation, and thermal feasibility constraints. Consequently, equipment thermal condition is transformed from an external monitoring output into an endogenous scheduling variable that actively governs generation dispatch, energy storage utilization, cooling management, AED charging, inspection routing, and equipment derating decisions. Through this integration, the proposed framework establishes a closed-loop interaction between aerial thermal monitoring and operational energy management, enabling geographically digitalized, thermally informed, and uncertainty-resilient coordination of integrated multi-energy systems. Therefore, the novelty of this work lies not in the individual use of reinforcement learning, thermographic inspection, or aerial monitoring technologies, but in the development of a unified thermal-feature-driven coordination framework in which visual thermal evidence serves as a real-time control signal for integrated energy management.

2. Methodology

2.1. AED-Enabled Thermal Monitoring Architecture for Priority-Driven Green Energy Hub

This section introduces a thermally constrained GEH that integrates an AED-based Temperature Monitoring Method, thereby directly limiting dispatch feasibility. As shown in Fig. 1, photovoltaic arrays and a Combined Heat and Power (CHP) unit serve as primary sources and are prioritized over grid imports under temperature constraints. Heating and cooling are supplied by conventional units, while electrical energy storage enhances flexibility.

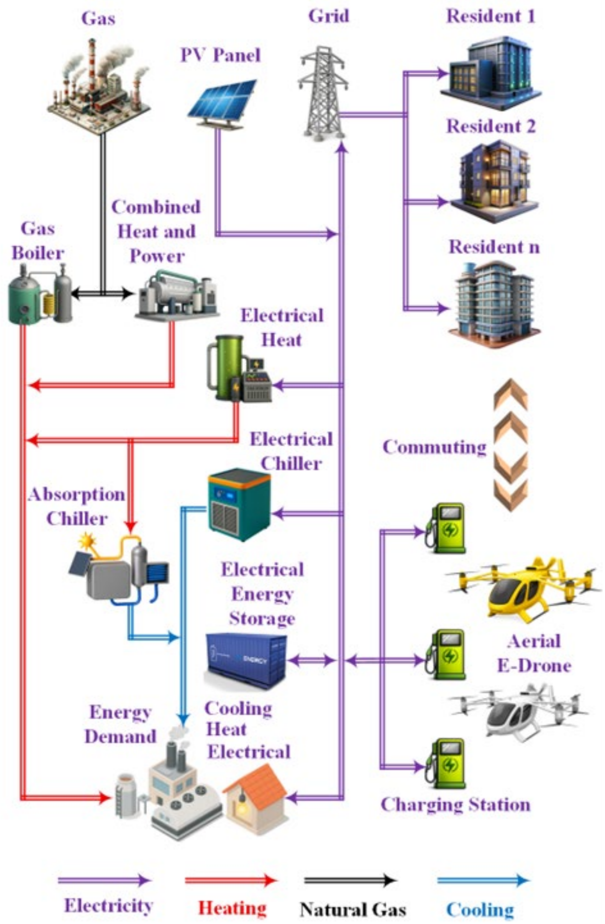

Fig. 1. Architecture of the thermally supervised GEH with AED coordination

The AED fleet enables both energy transfer and thermal inspection. Infrared data processed through morphological feature extraction and chromaticity analysis generate thermal risk coefficients that constrain generation and cooling performance. Dispatch follows a hierarchical order: maximize photovoltaic output, operate CHP within thermal limits, discharge storage, and import electricity from the grid if required. Coordinated scheduling minimizes the operating cost under thermal constraints. The framework transforms the GEH into a thermally adaptive system in which equipment condition information governs real-time energy decisions.

2.2. Thermal-Aware Objective Function Formulation

The framework, adapted from the energy conversion subsystems model, extends economic dispatch by integrating AED-based thermal monitoring to jointly minimize operating cost and temperature-induced equipment risk. The objective in Eq. (1) combines the GEH operating cost with a thermal risk index derived from AED observations. Economic components include fuel, grid transactions, and maintenance costs, as shown in Eqs. (2)-(4), while thermal deviations from safe limits are penalized (Mohammadian et al., 2026). For the Aerial e-drone Charging Station (AED CS), the net cost is defined as electricity purchase minus transaction revenue in Eq. (5). Monitoring-enhanced performance is further evaluated using the charging cost per unit of AED energy and the charging infrastructure utilization ratio in Eqs. (6) and (7).

$$\min J = C^{\mathrm{GEH}} + C^{\mathrm{AEDCS}} + \lambda \sum_{t=1}^{T} TR\, I_t \tag{1}$$

$$FC = \sum_{t=1}^{T} \left(G_t^{\mathrm{CHP}} + G_t^{\mathrm{GB}} \right) C_t^{\mathrm{gas}} \tag{2}$$

$$GC = \sum_{t=1}^{T} \left(E_t^{\mathrm{Grid,in}} C_t^{\mathrm{Grid,\,buy}} - E_t^{\mathrm{Grid,out}} C_t^{\mathrm{Grid,\,sell}} \right) \tag{3}$$

$$MC = \sum_{t=1}^{T} \left(E_t^{\mathrm{CHP}} + Q_t^{\mathrm{GB}} + Q_t^{\mathrm{EC}} + Q_t^{\mathrm{AC}} \right) C_t^{\mathrm{maint}} \tag{4}$$

$$TRI_t = \sum_{i \in \Omega_{\mathrm{com}}} w_i \left(T_{i,t} - T_i^{\mathrm{ref}} \right)^2 \tag{5}$$

$$C^{\mathrm{AEDCS}} = \sum_{t=1}^{T} E_t^{\mathrm{AEDCS}} C_t^{\mathrm{loc}} \tag{6}$$

$$C^{\mathrm{ch}} = \frac{\sum_t E_t^{\mathrm{ES,ch}} C_t^{\mathrm{loc}}}{\sum_t E_t^{\mathrm{ES,ch}}} \tag{7a}$$

$$U^{cs} = \frac{\sum_t E_t^{\mathrm{ES,ch}}}{E^{\mathrm{MRX}} \times T} \tag{7b}$$

2.2.1. Operational Constraints of Thermally Supervised GEH-AEDCS

In addition to the economic objective in Eqs. (1)-(7), the coordinated scheduling problem is subject to electricity, heat, storage, drone-energy, and thermal feasibility constraints. These constraints ensure that the actions selected by the learning agents remain physically feasible at each scheduling interval. The electrical power balance is expressed in Eq. (8).

$$P_t^{PV} + P_t^{CHP} + P_t^{ES,dis} + P_t^{Grid,in} + P_t^{AED,dis} = P_t^{load} + P_t^{ES,ch} + P_t^{Grid,out} + P_t^{AED,ch} + P_t^{EC} + P_t^{aux} \tag{8}$$

where photovoltaic generation, CHP generation, storage discharge, grid import, and AED discharge must supply the electrical demand, charging demand, grid export, electric chiller consumption, and auxiliary loads. The thermal energy balance is expressed in Eq.(9).

$$Q_t^{CHP} + Q_t^{GB} + Q_t^{EH} = Q_t^{heat} + Q_t^{AC} + Q_t^{loss} \tag{9}$$

where useful thermal output from the CHP, gas boiler, and electric heater satisfies heating demand, absorption cooling requirements, and thermal losses. The electrical storage state of charge evolves according to Eq. (10):

$$SOC_{t+1}^{ES} = SOC_t^{ES} + \eta_{ch}^{ES} P_t^{ES,ch} \Delta t - \frac{P_t^{ES,dis} \Delta t}{\eta_{dis}^{ES}} \tag{10}$$

subject to:

$$SOC_{min}^{ES} \leq SOC_t^{ES} \leq SOC_{max}^{ES} \text{ and: } \quad 0 \leq P_t^{ES,ch} \leq P_{max}^{ES,ch}, 0 \leq P_t^{ES,dis} \leq P_{max}^{ES,dis}$$

The aggregate AED energy state is modeled as Eq. (11).

$$E_{t+1}^{AED} = E_t^{AED} + \eta_{ch}^{AED} P_t^{AED,ch} \Delta t - \frac{P_t^{AED,dis} \Delta t}{\eta_{dis}^{AED}} - E_t^{flight} \tag{11}$$

with bounds: $E_{min}^{AED} \leq E_t^{AED} \leq E_{max}^{AED}$ the flight-energy requirement is constrained by Eq. (12).

$$E_t^{flight} = \kappa_1 d_t^{ins} + \kappa_2 t_t^{hover} + \kappa_3 n_t^{img} \tag{12}$$

$$E_t^{flight} \leq E_{max}^{flight}, t_t^{flight} \leq t_{max}^{flight}$$

where the AED flight energy depends on inspection distance, hovering duration, and imaging activity. To reflect thermal limitations, the CHP admissible output is reduced as a function of the thermal risk indicator: $0 \leq P_t^{CHP} \leq (1 - \rho_t^{TRI}) P_{max}^{CHP}$ where ρ_t^{TRI} is the thermal derating coefficient inferred from the monitored temperature condition. Similarly, the cooling devices satisfy: $0 \leq P_t^{EC} \leq P_{max}^{EC}, 0 \leq Q_t^{AC} \leq Q_{max}^{AC}(1 - \rho_t^{TRI})$ which captures the reduced allowable operation of the absorption chiller under elevated thermal stress. Finally, grid transactions remain bounded as: $0 \leq P_t^{Grid,in} \leq P_{max}^{Grid,in}, 0 \leq P_t^{Grid,out} \leq P_{max}^{Grid,out}$ and simultaneous excessive import/export behavior is prevented through the action design and market-clearing logic used by the coordinated controller. Together, these constraints define the feasible operating region of the thermally supervised GEH-AEDCS and clarify how thermal-state information enters both the reward mechanism and the dispatch admissibility set.

2.3. Morphological and Chromaticity Feature Extraction

The operational control of the integrated GEH-AEDCS platform is governed by two interacting decision-making entities, as illustrated in Fig. 2. One agent supervises the GEH and regulates dispatchable energy resources, while the second agent manages the AEDCS and determines aggregate bidirectional charging and discharging schedules for AED fleets. The thermal monitoring layer converts AED-acquired infrared frames into compact anomaly indicators for use by the scheduling agents. Let $I_t(x, y)$ denote the infrared temperature image acquired at time t. Before feature extraction, each frame is calibrated using the camera emissivity setting and background compensation, then normalized with respect to the admissible temperature interval of the inspected component in Eq. (13).

$$\tilde{I}_t(x,y) = \frac{I_t(x,y) - T_{min}^{ref}}{T_{max}^{ref} - T_{min}^{ref}} \tag{13}$$

where T_{min}^{ref} and T_{max}^{ref} are reference temperatures obtained under healthy operating conditions for the same equipment class.

To reduce sensor noise and isolated pixel artifacts, a median filter followed by a small-kernel Gaussian smoothing stage is applied. A hotspot mask $B_t(x,y)$ is then obtained by thresholding the normalized frame as in Eq. (14).

$$B_t(x,y) = \begin{cases} 1, & \tilde{I}_t(x,y) \geq \tau_T \\ 0, & \text{otherwise} \end{cases} \tag{14}$$

where τ_T is selected from baseline healthy-operation data using a percentile-based calibration rule.

Morphological analysis is then applied to the hotspot regions. Three structural descriptors are extracted, normalized hotspot area ratio A_t, contour irregularity C_t, and fragmentation index F_t. The area ratio represents the fraction of thermally abnormal pixels, the contour irregularity measures the deviation of hotspot boundaries from compact connected shapes, and the fragmentation index quantifies the number of disconnected hotspot regions after morphological cleaning. Based on these descriptors, the Morphological Deviation Index is defined as Eq. (15).

$$MDI_t = w_A \hat{A}_t + w_C \hat{C}_t + w_F \hat{F}_t \tag{15}$$

where $\hat{A}_t$, $\hat{C}_t$, and $\hat{F}_t$ are normalized deviations from their healthy reference values and $w_A + w_C + w_F = 1$.

In parallel, chromaticity analysis is performed on the pseudo-color thermal image derived from $I_t(x,y)$. The pseudo-color representation is mapped into a chromaticity feature space so that diffuse thermal spreading and uneven radiation patterns can be quantified even when hotspot shapes remain visually compact. Let $\mathbf{c}_t$ denote the chromaticity feature vector of the current image and $\mathbf{c}^{ref}$ the mean healthy-state chromaticity vector. The Chromaticity Anomaly Score is computed by Eq. (16).

$$CAS_t = \frac{1}{N} \sum_{k=1}^{N} \frac{|c_{t,k} - c_k^{ref}|}{\sigma_k^{ref} + \varepsilon} \tag{16}$$

where σ_k^{ref} is the healthy-state standard deviation of the k-th chromaticity component, N is the feature dimension, and ε is a small regularization constant used to avoid numerical instability.

To ensure compatibility with the reinforcement learning state and reward design, both MDI_t and CAS_t are normalized to the interval $[0,1]$ by min-max scaling over the calibration dataset. In addition, a moving-average temporal smoother is applied to suppress transient spikes caused by sensor motion, short-term reflections, or communication jitter during AED inspection. The resulting indicators are then incorporated into the learning process in two ways. First, they enrich the observation space by providing structural and chromatic thermal context beyond scalar temperature. Second, they influence the AEDCS reward in Eq. (9), allowing the controller to favor inspection and charging actions that improve anomaly observability while avoiding thermally unsafe operating conditions.

2.4. Markov Decision Process Formulation

System operation is modeled using two cooperative agents that interact with a stochastic environment. At each scheduling interval, agents observe the system states, apply control actions, and receive rewards, with policies optimized for the expected cumulative discounted return. Each subsystem operates autonomously but under coordinated decision-making. The observation space incorporates temperature-dependent information from AED monitoring, combining infrared-based morphological and chromaticity indicators with economic and energy variables. Global observations include shared market information and temporal variables, while the GEH local state augments load and generation data with thermal risk indices and derating factors. The AEDCS local state incorporates cumulative energy constraints and anomaly metrics to support thermally informed policy learning.

The action space explicitly incorporates thermal constraints into dispatch. GEH actions cover storage use, combined heat and power output, electric heater operation, and absorption chiller control. AEDCS actions include charging, discharging, and inspection-related adjustments such as trajectory changes and imaging-mode selection. State transitions remain stochastic owing to uncertainties in energy demand, renewables, and AED availability, with dynamics learned from interaction data. The reward structure combines economic objectives with thermal stability: GEH rewards penalize cost and thermal risk, while AEDCS rewards balance charging revenue with inspection quality and flight-energy consumption as Eqs. (17)-(18).

$$r_t^{\text{GEH}} = -C_t^{\text{GEH}} - \lambda_1 \text{TRI}_t \tag{17}$$

$$r_t^{\text{AEDCS}} = -C_t^{\text{AEDCS}} + \lambda_2 \text{MDI}_t + \lambda_3 \text{CAS}_t - \lambda_4 E_t^{\text{flight}} \tag{18}$$

where Morphological Deviation Index (MDI) and Chromaticity Anomaly Score (CAS) provide learning signals for thermally informed inspection planning.

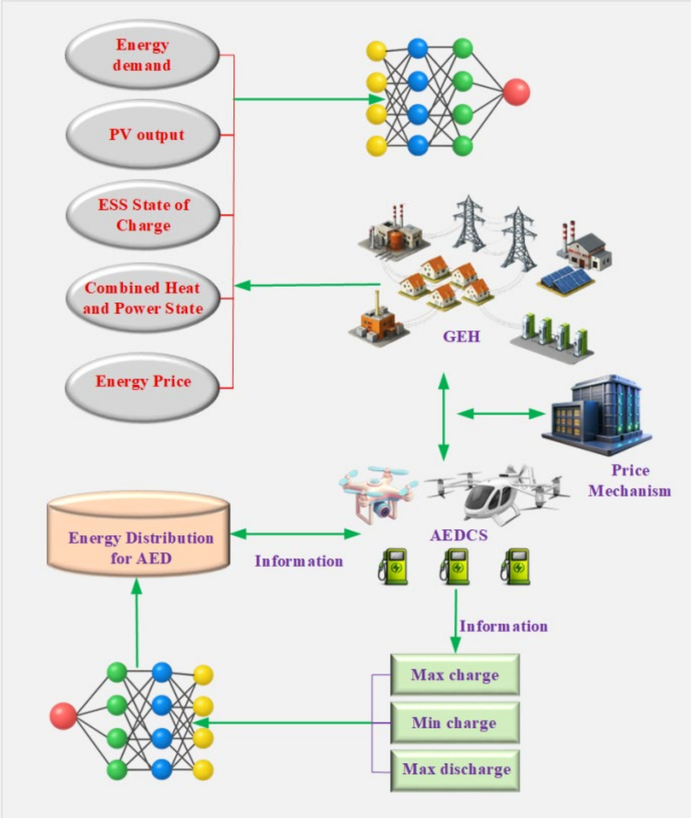

Fig. 2. Control hierarchy of GEH-AEDCS platform

2.5. Thermal-State-Aware FRL Framework

Because the GEH dispatch decisions are continuous, the Twin Delayed Deep Deterministic Policy Gradient (TD3) algorithm is adopted to improve training stability and mitigate overestimation bias through twin critics and delayed policy updates. The entropy-regularized objective function is defined in Eq. (19).

$$J(\pi) = \sum_{t=0}^{\infty} \mathbb{E}_{(s_t,a_t)\sim\pi}\left[r(s_t,a_t) + \alpha H(\pi(\cdot| s_t))\right] \tag{19}$$

with policy entropy given by Eq. (20).

$$H(\pi(\cdot| s_t)) = -\log \pi(\cdot| s_t) \tag{20}$$

The corresponding soft action-value function is expressed in Eq. (21).

$$Q(s,a) = \mathbb{E}_\pi\left[\sum_{t=0}^{\infty} \gamma^t \left(r(s_t,a_t) + \alpha H(\pi(\cdot| s_t))\right) | s_0 = s, a_0 = a\right] \tag{21}$$

and the Bellman optimality relation is given in Eq. (22).

$$Q^*(s,a) = r(s_t,a_t) + \gamma \mathbb{E}_{s_{t+1},a_{t+1}}\left[Q(s_{t+1},a_{t+1}) - \alpha \log \pi(\cdot| s_{t+1})\right] \tag{22}$$

The optimal policy is obtained using Eq. (23).

$$\pi^*(\cdot| s) = \arg\max_{\pi} \mathbb{E}_{a\sim\pi}\left[Q(s_t,a) + \alpha H(\pi(\cdot| s_t))\right] \tag{23}$$

To address non-stationarity and heterogeneous agent roles, a Feudal Reinforcement Learning (FRL) framework is employed instead of independent TD3 or symmetric CTDE approaches. The hierarchical leader-follower interaction is modeled as a bi-level optimization problem as Eq. (24).

$$\max_{\pi_1\in\Pi_1}\left\{\mathbb{E}_{\pi_1,\pi_2^*}\left[\sum_{t=1}^{\infty} \gamma_1^t r_{1,t}\right]\right\} \text{s.t. } \pi_2^* = \arg\max_{\pi_2\in\Pi_2}\left\{\mathbb{E}_{\pi_1,\pi_2}\left[\sum_{t=1}^{\infty} \gamma_2^t r_{2,t}\right]\right\} \tag{24}$$

where the upper-level agent governs thermally constrained energy dispatch, and the lower-level agent optimizes AED inspection and charging strategies in response. Centralized offline training with global observations is combined with decentralized execution, allowing stable convergence under thermal uncertainty and coordinated multi-agent scheduling.

3. Results

The thermally adaptive FRL framework was tested on a simulated GEH-AEDCS platform over a 24-hour horizon. The objective is to balance local generation and cost reduction under temperature constraints through real-time scheduling. The environment included equipment temperature dynamics and AED monitoring, with thermal data converted into morphological deviation and chromaticity indices that adjusted generation limits and efficiencies. Demand and photovoltaic datasets, as well as all remaining parameters, followed established references. The platform was implemented in Python, with training and thermal preprocessing based on prior studies. This section is adapted from Refs. (Mohamadi et al., 2025b; Zare et al., 2026). Fig. 3 provides representative daily electricity and heat profiles.

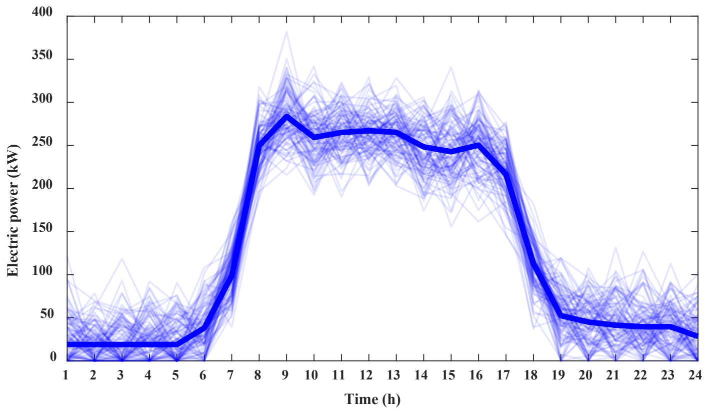

(a) Electricity

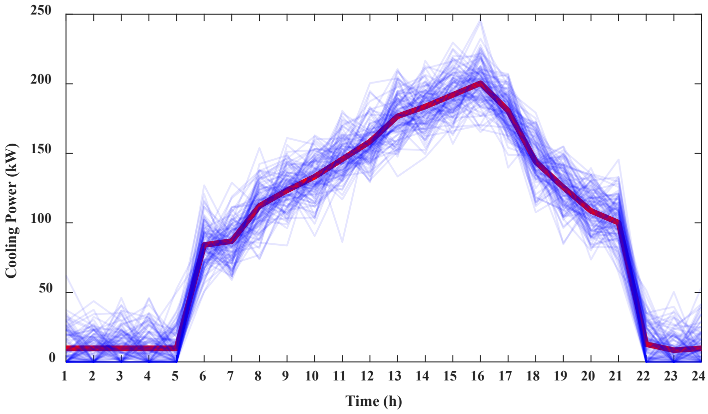

(b) Heat profiles

Fig. 3. Typical daily

3.1. Algorithmic Benchmarking under Thermal-Constrained Generation-Priority Strategy

The proposed FRL framework was benchmarked against TD3, D4PG, and MILP-based approaches under thermally constrained operating conditions. Training was conducted over 2600 daily episodes using embedded thermal indicators (TRI, MDI, CAS). Performance was evaluated in terms of operating cost, renewable energy priority, and thermal risk, demonstrating the ability of the proposed framework to simultaneously balance economic and thermal objectives.

3.2. Convergence Characteristics of Competing Learning Frameworks

All algorithms were trained for 2600 episodes using identical random seeds. As shown in Fig. 4, FRL achieves the highest and most stable reward, outperforming TD3 and D4PG, with faster convergence and lower variance under thermally constrained operation.

3.3. Generalization Performance under 30-Day Operational Horizon

The FRL framework demonstrated strong generalization capability over a 30-day horizon, as reflected by the accumulated operating-cost trends in Fig. 5. The FRL framework remained close to Perfect-MILP solution, achieving a mean daily cost of 214.6 USD compared with 205.3 USD for Perfect-MILP (approximately 4 % deviation), while reducing the operating cost by approximately 8 % compared with TD3 (232.9 USD) and 15 % compared with D4PG (251.4 USD). These outcomes align with prior convergence behavior. Execution time further distinguished the methods: FRL required 0.63 s per step, substantially faster than Perfect-MILP (7.92 s) and stochastic optimization (12.37 s), illustrating the efficiency gap between neural inference and iterative optimization. TD3 and D4PG remained slightly faster per step (0.48 s and 0.44 s) but produced higher operating costs. The combined results indicate that FRL achieves the most effective balance between economic performance, thermal feasibility, and computational efficiency.

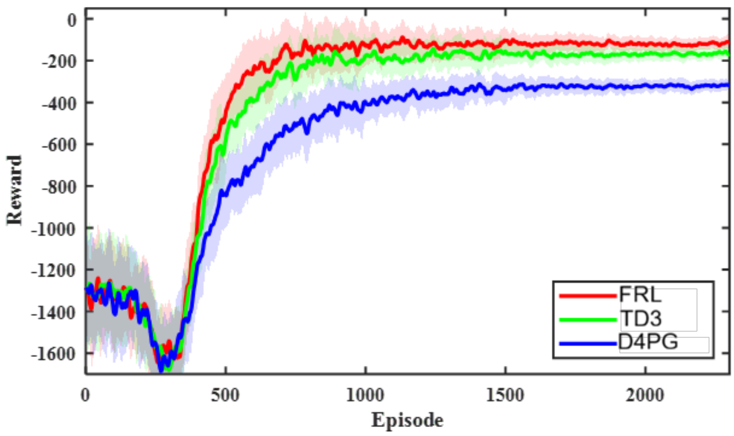

Fig. 4. Convergence behavior of FRL, TD3, and D4PG under thermally constrained dispatch

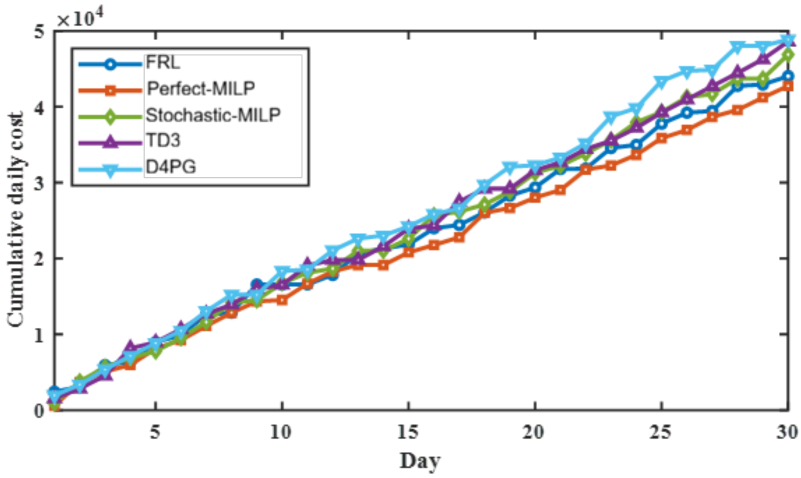

Fig. 5. Thirty-day cumulative operating expense comparison across control strategies

3.4. Coordinated GEH-AED Operation with Embedded Thermal Surveillance

The Feudal Reinforcement Learning controller was further evaluated under two seasonal conditions from the test dataset. The summer profile includes abundant solar availability and high cooling demand, while the winter profile features limited solar contribution and dominant heating demand. A temperature-monitoring method for Power Equipment is incorporated into the GEH supervisory layer, where the thermal states of critical assets are inferred from temporal temperature-gradient features and chromaticity analysis of infrared imagery collected by AED units. These thermal indicators penalize excessive equipment heating and restrict system operation near unsafe temperature thresholds.

3.4.1. Seasonal Operation of Green Energy Hub

Fig. 6 illustrates that off-peak electricity demand is supplied primarily by the utility grid while the energy storage system is simultaneously charged. Whereas daytime demand is primarily supplied by the CHP unit, with storage and AED near-peak support. AED charging aligns with high photovoltaic output and acceptable thermal conditions. Cooling is managed by the electric chiller at night and the absorption chiller during thermally stable daytime periods.

3.4.2. Generalization performance under 30-day operational horizon

The FRL framework demonstrated strong generalization capability over a 30-day horizon, as reflected by the accumulated operating-cost trends in Fig. 5. The FRL framework remained close to Perfect-MILP solution, achieving a mean daily cost of 214.6 USD compared with 205.3 USD for Perfect-MILP (approximately 4 % deviation), while reducing the operating cost by approximately 8 % compared with TD3 (232.9 USD) and 15 % compared with D4PG (251.4 USD). These outcomes align with prior convergence behavior. Execution time further distinguished the methods: FRL required 0.63 s per step, substantially faster than Perfect-MILP (7.92 s) and stochastic optimization (12.37 s), illustrating the efficiency gap between neural inference and iterative optimization. TD3 and D4PG remained slightly faster per step (0.48 s and 0.44 s) but produced higher operating costs. The combined results indicate that FRL achieves the most effective balance between economic performance, thermal feasibility, and computational efficiency.

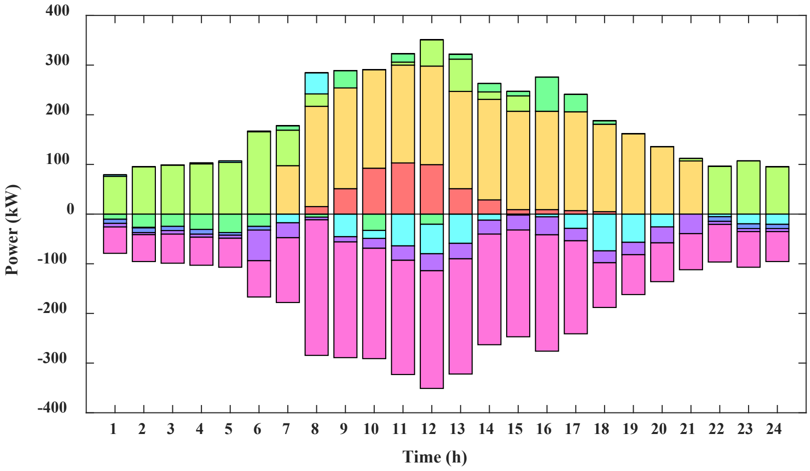

(a) Electricity

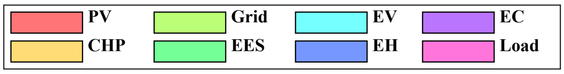

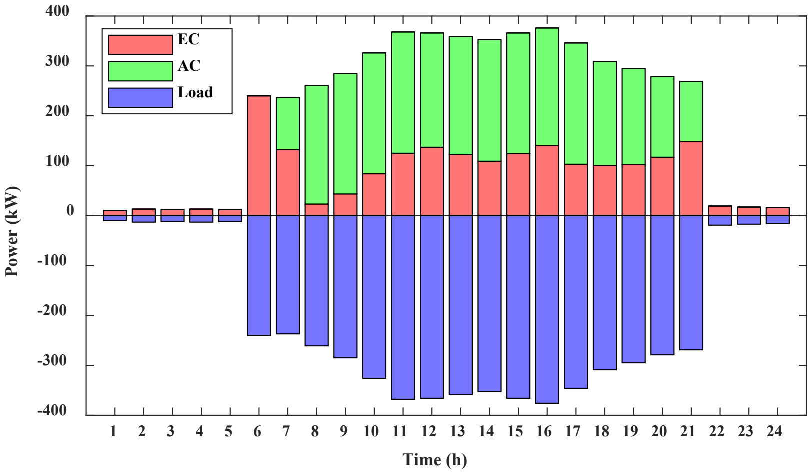

(b) Cooling dispatch under thermal supervision

Fig. 6. Off-peak electricity demand supplied by the utility grid while charging the energy storage system

3.4.3. AED charging behavior

Fig. 8 shows the AEDCS charging scheduling during a typical summer day. Charging demand peaks between 8:00 and 14:00, with a secondary peak in the late afternoon. Early charging demand is supported by coordinated AED discharge and GEH generation. Around midday, lower electricity tariffs permit partial grid utilization while satisfying the imposed thermal constraints.

Fig. 9 illustrates the energy allocation strategy adopted for the AED fleet. The AED units with early departures receive priority, while those with longer dwelling times receive moderated charging rates. Discharge-enabled vehicles inject energy upon arrival when temperature thresholds are satisfied.

Three configuration scenarios are considered to quantify the economic benefits of the proposed coordination strategy: Scenario A: immediate maximum-rate charging. Scenario B: coordinated charging without interzonal transfer, Scenario C: fully coordinated cross-spatiotemporal transfer. Table 1 summarizes the operating costs over the 100-day evaluation period. Scenario C achieves the lowest operating cost at 29,934 USD, compared with 32,797 USD in Scenario A, a reduction of approximately 9 %. Maintenance costs decrease as the level of coordination increases. Specifically, the AEDCS maintenance expenditure decreases from 8,054 USD in Scenario A to 6,556 USD in Scenario C owing to moderated thermal cycling confirmed by morphological and chromaticity-based diagnostics.

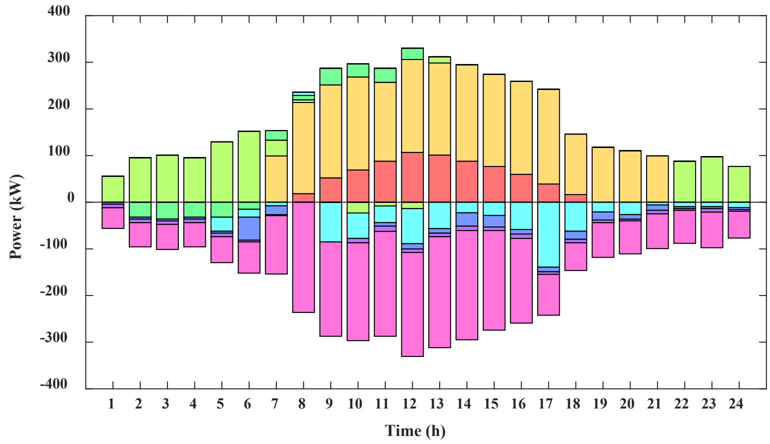

(a) Electricity

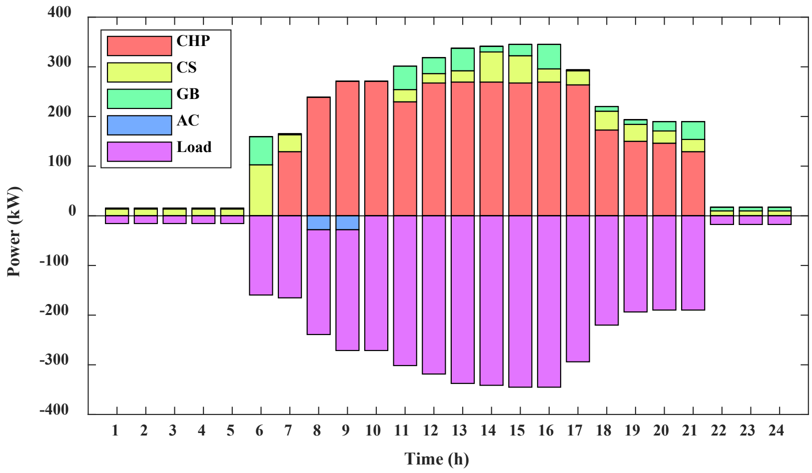

(b) Heating coordination results

Fig. 7. Winter power and heat supply from grid, battery, and CHP

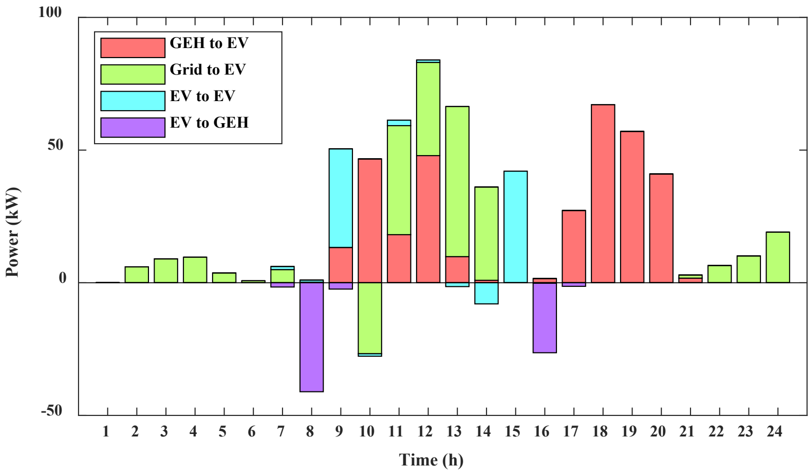

Fig. 8. AEDCS charging profile on a representative summer day

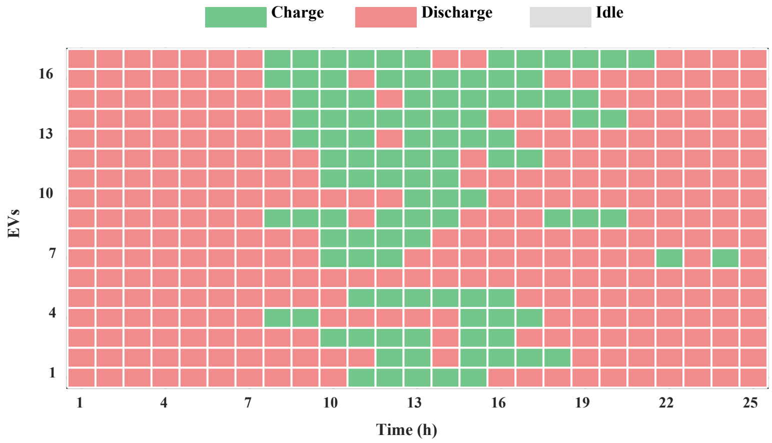

Fig. 9. Energy allocation dynamics based on departure priority

Table 1. Cost decomposition under thermally constrained operational scenarios (USD)

Scenario	Integrated system cost (USD)	GEH maintenance expenditure (USD)	AEDCS maintenance expenditure (USD)
Scenario A	32,797	24,743	8,054
Scenario B	31,254	24,141	7,113
Scenario C	29,934	23,378	6,556

3.5. Thermal Monitoring Results

To further validate the effectiveness of the proposed temperature-monitoring and feature-extraction framework, this section presents representative visual outputs from the AED-based inspection process. These results demonstrate how raw infrared observations are transformed into meaningful thermal indicators through morphological and chromaticity analyses.

3.5.1. Infrared thermal imaging from AED inspection

Fig. 10 illustrates a representative infrared thermal image captured by the AED system during inspection of critical GEH components. The acquired image provides a spatially continuous temperature distribution, in contrast to conventional point-based sensing approaches. Distinct localized hotspots are observed in regions associated with high operational stress, including transformer units and CHP-related components. These thermal concentrations indicate potential overheating risks and efficiency degradation. The spatially resolved temperature information enables the early identification of abnormal regions before system-level failures occur. This form of monitoring establishes the foundation for integrating temperature as a dynamic state variable within the control framework rather than treating it as a passive diagnostic output.

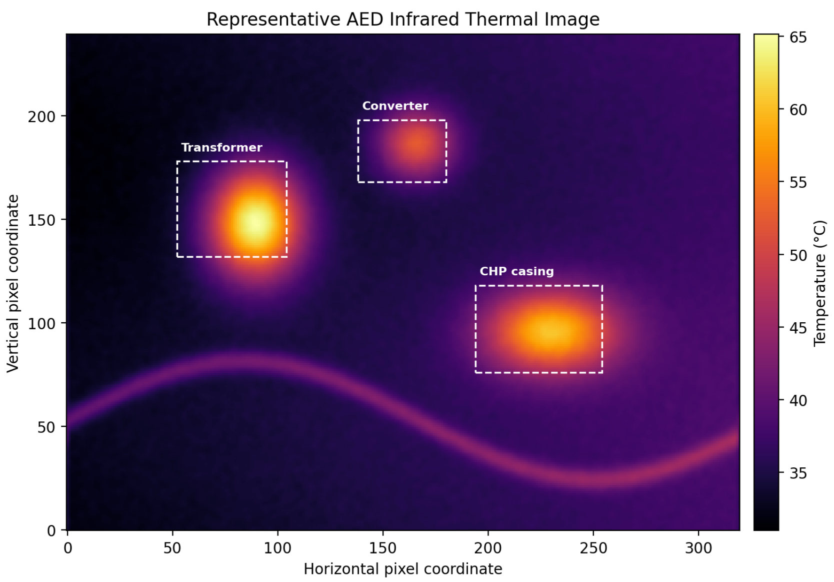

Fig. 10. AED infrared thermal image showing temperature distribution and hotspots

3.5.2. Morphological feature extraction

Fig. 11 presents the morphological feature map derived from the infrared thermal image. The extraction process identifies structural characteristics of thermal distributions, including hotspot contours, boundary irregularities, and spatial connectivity of high-temperature regions. The Morphological Deviation Index (MDI) is computed by quantifying deviations in these structures relative to normal operating patterns. Specifically, irregular contour expansion, fragmentation of thermal regions, and steep spatial gradients are interpreted as indicators of abnormal system behavior. Compared with raw temperature values, morphological features provide a higher-level representation of thermal conditions by capturing the geometry and evolution of heat concentration. This allows the control system to detect not only extreme temperatures but also structurally abnormal thermal configurations that precede critical events.

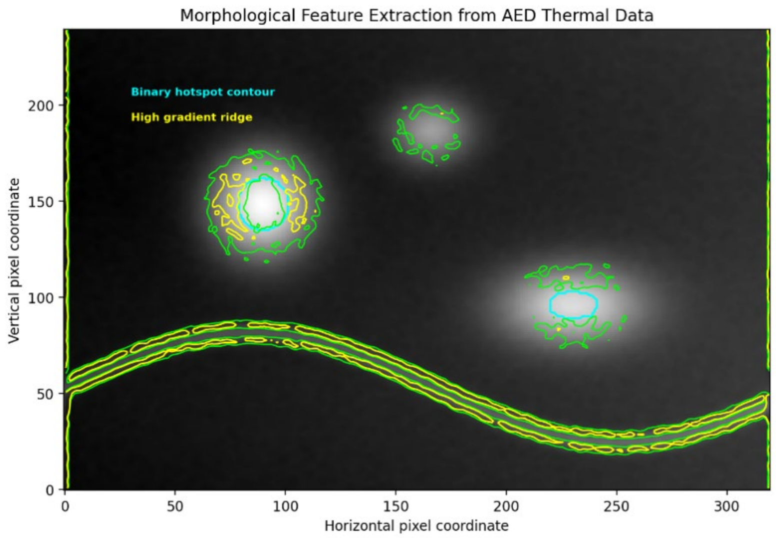

Fig. 11. Morphological feature extraction highlighting hotspot contours and structural thermal deviations

3.5.3. Chromaticity-based thermal anomaly analysis

Fig. 12 presents the chromaticity analysis of the same thermal image. By transforming infrared intensity distributions into color-space representations, the proposed method captures subtle variations in thermal radiation that are not readily observable in grayscale or raw thermal images.

The Chromaticity Anomaly Score (CAS) is derived from deviations in color distribution, reflecting abnormal heat dispersion, uneven thermal diffusion and early-stage degradation signals. Compared with morphological analysis alone, chromaticity analysis improves sensitivity to gradual and diffuse anomalies, thereby enhancing early detection capability.

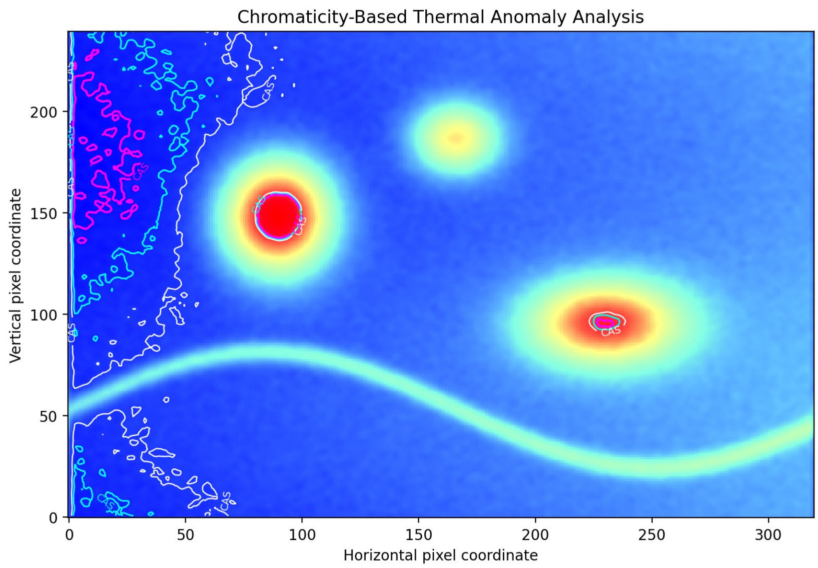

Fig. 12. Chromaticity-based analysis illustrating thermal diffusion patterns and anomaly regions

4. Discussion

The results in Table 2 indicate that integrating AED-based thermal monitoring with morphological and chromaticity features significantly reduces system cost, maintenance, and thermal risk compared to baseline configurations. The full feature-based approach enables earlier anomaly detection, resulting in fewer hotspots and improved component efficiency. As illustrated in Fig. 13, the Thermal Risk Index exhibits lower variability and greater stability under thermally constrained operation.

Table 2. Quantitative impact of AED-based thermal monitoring and feature-driven supervision (100-day horizon)

Metric	No Monitoring	Temperature Only	Full Feature-Based (Proposed)
Integrated System Cost (USD)	33,842	31,487	29,934
GEH Maintenance Cost (USD)	25,918	24,032	23,378
AEDCS Maintenance Cost (USD)	8,224	7,284	6,556
Mean Thermal Risk Index (TRI)	0.184	0.129	0.071
CHP Forced Derating Events (count)	47	29	12
Transformer Hotspots (count)	32	19	8
EC Efficiency Loss (%)	6.8	4.2	1.7
Absorption Cooling Deviation (%)	5.9	3.6	1.4
Anomaly Detection Accuracy (%)	71	82	94
AED Inspection Coverage (%)	0	62	96

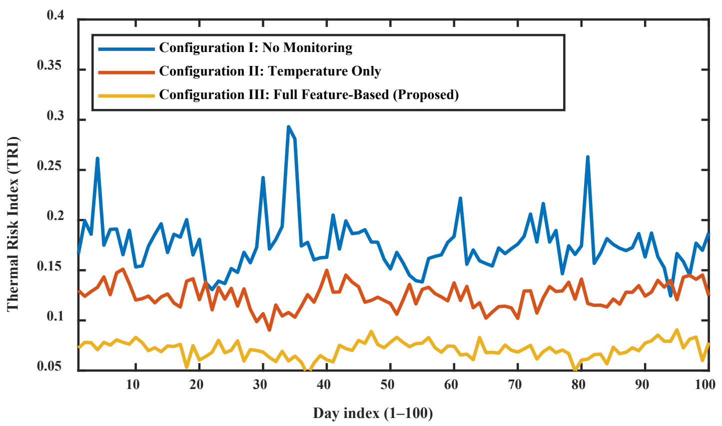

Fig. 13. Temporal evolution of thermal risk index under different monitoring configurations

5. Conclusion

This study demonstrates that thermal monitoring can be integrated directly into energy management rather than being treated as a separate diagnostic task. By combining AED-based inspection, morphological feature extraction, chromaticity analysis, and hierarchical reinforcement learning, the proposed framework improves both economic performance and thermal safety in the GEH-AEDCS platform. The results indicate lower operating costs, lower thermal risk, fewer forced derating events, and higher inspection coverage than the benchmark methods. From a managerial standpoint, the paper redefines how decisions should be made in four areas. First, managers should revise dispatch decisions based not only on cost and demand, but also on real-time thermal conditions of critical equipment. Second, maintenance decisions should shift from periodic inspection to predictive intervention based on thermal-risk signals. Third, equipment loading decisions should be adjusted dynamically to avoid overheating and efficiency losses in CHP, cooling, and energy-storage units. Fourth, AED fleets should be managed not only as mobile energy assets but also as active inspection resources within the overall system operation. In this sense, the paper suggests that managers should transition from static, cost-centered operations to condition-aware, risk-responsive, and inspection-integrated decision-making. The main limitation of this study is that the proposed framework has been validated only in a simulated environment. Future work should validate the proposed framework using real infrared inspection data and practical multi-hub energy systems.

Author Contributions

Yuze Chen contributed to conceptualization, methodology, experimental design, data analysis and writing of the original draft. Shanyi Xie contributed to technical support, data validation, review writing, editing and visualization. Kai Zhang contributed to investigation, experimentation, data collection, data analysis, writing, review and editing. Ying Fan contributed to investigation, experimentation, data collection, data analysis, writing, review and editing. Gang Zhou contributed to supervision, project administration, writing, review and editing, final manuscript review and approval.

Funding

This research was financially supported by Guangdong Power Grid Co., Ltd. under the research project entitled "Research on Distribution Network Video Integrated Monitoring Device and Video Intelligent Analysis Technology Based on Electric Hong IoT Operating System" (Project No. GDKJXM20240268). The financial support provided by this project enabled the design and implementation of the research, including the development of the experimental framework, data collection, data analysis, technical validation, and manuscript preparation. The funding organization provided financial resources to support the execution of the project; however, it had no influence on the interpretation of the results, the conclusions drawn, or the decision to submit the manuscript for publication. The authors gratefully acknowledge Guangdong Power Grid Co., Ltd. for its support of this research.

Institutional Review Board Statement

Not applicable.

Declaration of Artificial Intelligence (AI) Tools

The authors used ChatGPT-5.2 solely for language editing and to improve readability. The authors did not use any AI tools for generating scientific content, equations, analyses, or conceptual material. The authors reviewed and verified all content and take full responsibility for the accuracy and integrity of the manuscript.

References

Andreou, A., Mavromoustakis, C. X., Batalla, J. M., Markakis, E. K., Mastorakis, G., and Mumtaz, S. (2023). UAV trajectory optimisation in smart cities using modified A* algorithm combined with haversine and vincenty formulas. *IEEE Transactions on Vehicular Technology*, 72(8), 9757-9769. doi: 10.1109/TVT.2023.327XXXX

Bansal, A., Agrawal, N., Singh, K., Li, C.-P., and Mumtaz, S. (2023). RIS selection scheme for UAV-based multi-RIS-aided multiuser downlink network with imperfect and outdated CSI. *IEEE Transactions on Communications,* 71(8), 4650-4664. doi: 10.1109/TCOMM.2023.327XXXX

Bashyal, A., Boroukhian, T., Veerachanchai, P., Naransukh, M., and Wicaksono, H. (2025). Multi-agent deep reinforcement learning based demand response and energy management for heavy industries with discrete manufacturing systems. *Applied Energy*, 392, 125990. https://doi.org/10.1016/j.apenergy.2025.125990

Chen, Y., Xia, R., Yang, K., and Zou, K. (2025). Dual degradation image inpainting method via adaptive feature fusion and U-net network. *Applied Soft Computing*, 174, 113010. https://doi.org/10.1016/j.asoc.2025.113010

Deng, J., Wang, X., and Meng, F. (2025). Multi-agent deep reinforcement learning for Smart building energy management with chance constraints. *Energy and Buildings*, 331, 115408. https://doi.org/10.1016/j.enbuild.2025.115408

Franzoso, A., Fambri, G., and Badami, M. (2026). Deep reinforcement learning control architectures for industrial multi-energy systems: from single-agent to hierarchical multi-agents. *Energy Conversion and Management*, 350, 120963. https://doi.org/10.1016/j.enconman.2025.120963

Kardaris, N., Mermigkas, P., Moustris, G., Tzafestas, C., and Maragos, P. (2025). Automated Thermal Fault Detection in Ultra-High Voltage Substation Equipment. *IFAC-PapersOnLine*, 59(9), 73–78. https://doi.org/10.1016/j.ifacol.2025.08.115

Li, Y., Zhao, B., Li, Y., Long, C., Li, S., Dong, Z., and Shahidehpour, M. (2025). Safe-AutoSAC: AutoML-enhanced safe deep reinforcement learning for integrated energy system scheduling with multi-channel informer forecasting and electric vehicle demand response. *Applied Energy*, 399, 126468. https://doi.org/10.1016/j.apenergy.2025.126468

Li, Z., Qin, Q., Yang, Y., Mai, X., Ieiri, Y., and Yoshie, O. (2025). An enhanced substation equipment detection method based on distributed federated learning. *International Journal of Electrical Power & Energy Systems*, 166, 110547. https://doi.org/10.1016/j.ijepes.2025.110547

Luo, Y., and Jiang, C. (2025). A multi-agent reinforcement learning with markov decision process for integrated energy systems in low-carbon economic. *Alexandria Engineering Journal*, 131(17_supplement_2), 245–262. https://doi.org/10.1016/j.aej.2025.10.010

Mohamadi, B., Dejamkhooy, A., Shayeghi, H., Zare, P., and Mohammadian, A. (2025a). Cooperative computing synergistic in hydrogen-based city energy community complementary clusters considering dual sustainable transportation and stakeholder social welfare. *Sustainable Computing: Informatics and Systems*, 48, 101237. https://doi.org/10.1016/J.SUSCOM.2025.101237

Mohamadi, B., Dejamkhooy, A., Shayeghi, H., Zare, P., and Mohammadian, A. (2025b). Cooperative Computing Synergistic in Hydrogen-Based City Energy Community Complementary Clusters Considering Dual Sustainable Transportation and Stakeholder Social Welfare. *Sustainable Computing: Informatics and Systems*, 101237. https://doi.org/10.1016/J.SUSCOM.2025.101237

Mohammadian, A., Dejamkhooy, A., SeyedShenava, S., Zare, P., and Mohamadi, B. (2026). Cross-Sectoral Synergy Policy in Climate-Neutral Sustainable Cities with Eco-Friendly Public Transportation Fleets and Hydrogen-Pivoted Multi-Energy Transactions. *Energy*, 140296. https://doi.org/10.1016/j.energy.2026.140296

Qi, H., Ma, W., and Zhao, B. (2025). Federated heterogeneous multi-agent deep reinforcement learning-based attack resilience scheduling for heterogeneous multi-integrated energy system. *Energy Reports*, 14(4), 116–127. https://doi.org/10.1016/j.egyr.2025.05.085

Shayeghi, H., Mohamadi, B., and Bizon, N. (2026). Spatiotemporal optimization of peer-to-peer energy transactions in sustainable ecosystem clusters with blue-green hydrogen integration and e-transportable storage under carbon neutrality goals. *International Journal of Hydrogen Energy*, 197, 152539. https://doi.org/10.1016/J.IJHYDENE.2025.152539

Shayeghi, H., Mohamadi, B., Younesi, A., Sadr, S., and Siano, P. (2026). Cooperative stochastic energy management of multi smart home microgrids joint with modern distribution network. *Scientific Reports 2026*. https://doi.org/10.1038/s41598-025-34945-w

Toquica, D., Agbossou, K., and Henao, N. (2025). Multi-agent reinforcement learning for energy management in microgrids with shared hydrogen storage. *International Journal of Hydrogen Energy*, 144, 1019–1027. https://doi.org/10.1016/j.ijhydene.2025.01.413

Wang, R., Zhou, Z., Li, S., and Zhang, Z. (2025). Advances and challenges in infrared-visible image fusion: a comprehensive review of techniques and applications. *Artificial Intelligence Review 2025 59:1*, 59(1), 18. https://doi.org/10.1007/s10462-025-11426-0

Wei, Y., Cheng, Y., Liao, H., Wang, H., and Wang, K. (2025). Fleet Service Reliability Analysis of Self-Service Systems Subject to Failure-Induced Demand Switching and a Two-Dimensional Inspection and Maintenance Policy. *IEEE Transactions on Automation Science and Engineering*, 22, 10029–10044. https://doi.org/10.1109/TASE.2024.3516049

Wei, Y., Li, A., Li, Y., Cheng, Y., and Liao, H. (2026). An optimal predictive inspection and maintenance policy for a multi-state system: A belief-based SMDP approach. *Reliability Engineering and System Safety*, 265(Part B), 111497. https://doi.org/10.1016/j.ress.2025.111497

Wei, Y. and Cheng, Y. (2025). An optimal two-dimensional maintenance policy for self-service systems with multi-task demands and subject to competing sudden and deterioration-induced failures. *Reliability Engineering and System Safety*, 255, 110628. https://doi.org/10.1016/j.ress.2024.110628

Zare, P., Shayeghi, H., SeyedShenava, S., and Mohamadi, B. (2026). Interactive Scheduling for Climate-Neutral Sustainable Cities via Carbon Capture-Enabled Virtual Energy Communities Considering Digital-Social Welfare and Joint Certificate Trading. *Sustainable Cities and Society*, 107208. https://doi.org/10.1016/j.scs.2026.107208

Zhang, F., Hu, H., and Wang, Y. (2023). Infrared image enhancement based on adaptive non-local filter and local contrast. *Optik*, 292, 171407. https://doi.org/10.1016/j.ijleo.2023.171407

Zhang, P., Yang, T., Yan, H., Zhu, Y., Hu, Y., Zeng, D., and Liu, J. (2025). Two-level deep reinforcement learning approach for energy management of integrated energy system considering deep peak shaving for combined heat and power and coordinated scheduling of electric vehicles. *Applied Thermal Engineering*, 275, 126773. https://doi.org/10.1016/j.applthermaleng.2025.126773

Zhou, X., Wu, X., Bao, L., Yin, H., Jiang, Q., and Zhang, J. (2025). AGFNet: Adaptive Gated Fusion Network for RGB-T Semantic Segmentation. *IEEE Transactions on Intelligent Transportation Systems*, 26(5), 6477–6492. https://doi.org/10.1109/TITS.2025.3528064

Yuze Chen, master, current engineer of Electric Power Research Institute of Guangdong Power Grid Co., Ltd. His research expertise includes computer vision and multimodal large models. He maintains close cooperation with Shanghai Jiao Tong University and works on visible light image recognition. A number of high-impact papers have been published in Computer Vision and Pattern Recognition (CVPR).

Shanyi Xie, master, current senior engineer of Electric Power Research Institute of Guangdong Power Grid Co., Ltd. His research expertise includes electrical engineering and communication engineering. He has long been engaged in the research, application, and innovation of key technologies for electric power systems, focusing on improving grid communication and electrical safety.

Kai Zhang, master, current engineer of Electric Power Research Institute of Guangdong Power Grid Co., Ltd. His research expertise includes Internet of Things (IoT) and Mobile Computing. He maintains close cooperation with Nanjing University and is committed to research on intelligent sensing and mobile power grid applications. A number of high-impact papers have been published in Proceedings of the ACM on interactive, mobile, wearable and ubiquitous technologies.

Ying Fan, master, current senior engineer of Electric Power Research Institute of Guangdong Power Grid Co., Ltd. His research expertise includes communication engineering and electrical engineering. He is devoted to research on power communication networks and smart grid technology, contributing actively to the digital transformation of power systems.

Gang Zhou, master, current senior engineer of Electric Power Research Institute of Guangdong Power Grid Co., Ltd. His research expertise includes computer architecture and electrical engineering. He has long been devoted to developing and managing innovative electric power engineering projects, with a focus on new computing architectures for the grid.